Lowering Charge Transfer Barrier of $LiMn_2O_4$ via Nickel Surface Doping to Enhance Li^+ Intercalation Kinetics at Subzero Temperatures

Wei Zhang,[†] Xiaoli Sun,[‡] Yuxin Tang,[†] Huarong Xia,[†] Yi Zeng,[†] Liang Qiao,[†] Zhiqiang Zhu,[†] Zhisheng Lv,[†] Yanyan Zhang,[†] Xiang Ge,[†] Shibo Xi,[§] Zhiguo Wang,[‡] Yonghua Du,*[,§] and Xiaodong Chen*[,†]

[†] Innovative Centre for Flexible Devices, School of Materials Science and Engineering, Nanyang Technological University, 50 Nanyang Avenue, Singapore 639798, Singapore

[‡] School of Electronics Science and Engineering, University of Electronic Science and Technology of China, Chengdu, 610054, P.R. China

[§] Institute of Chemical and Engineering Sciences, 1 Pesek Road, Jurong Island, Singapore 627833, Singapore

Supporting Information Placeholder

ABSTRACT: Sluggish interfacial kinetics leading to considerable loss of energy and power capabilities at subzero temperatures is still a big challenge to overcome for Li-ion batteries operating under extreme environmental conditions. Herein, using $LiMn_2O_4$ as the model system, we demonstrated that nickel surface doping to construct a new interface owning lower charge-transfer energy barrier, could effectively facilitate the interfacial process and inhibit the capacity loss with decreased temperature. Detailed investigations on the charge transfer process via electrochemical impedance spectroscopy and density functional theory calculation, indicate that the interfacial chemistry tuning could effectively lower the activation energy of charge transfer process by nearly 20%, endowing the cells with ~75.4% capacity at -30 °C, far surpassing the hardly discharged unmodified counterpart. This control of surface chemistry to tune interfacial dynamics proposes insights or design ideas for batteries to well survive under thermal extremes.

Substantially reduced energy and power capabilities of Li-ion batteries (LIBs) at subzero temperatures are among the main hindrances for their wide acceptance in high-altitude, aerospace and military applications as well as electrical vehicles in cold regions,[1] despite the great success at room temperature.[2] The poor performances are largely ascribed to the exponentially increased resistance of cells caused by diminished transport properties of electrolyte, sluggish charge transfer process and slow Li diffusion in the bulk materials at low temperatures.[3] Current efforts mainly focused on electrolyte and electrode,[4] such as using ethyl acetate with low viscosity (~0.45 cP) and melting point (~-84 °C) as co-solvent for ethylene carbonate to reduce the liquidus temperatures of the electrolyte,[5] or adopting nanostructures to short Li-ion diffusion path lengths in the bulk of active materials, but at the cost of hard to form a stable solid-electrolyte interphase to preserve a long cycle life both at elevated temperatures.

Unfortunately, the true limitation of low-temperature performance is likely originated from the interfacial process, typically, substantially increased charge transfer resistance.[6] According to the relationship the charge transfer resistance (R_{ct}) follows based on thermally activated process (Equation 1),[7]

$$\frac{1}{R_{ct}} = A_0 e^{-E_a/RT} \quad (1)$$

where A_o is a constant, E_a represents the activation energy, T means the temperature in Kelvin and R is known as the gas constant, the change of charge transfer resistance with temperature is largely determined by the activation energy (Scheme 1a,b). Therefore, the key to addressing the sluggish interfacial kinetics lies in lowering the corresponding threshold energy.

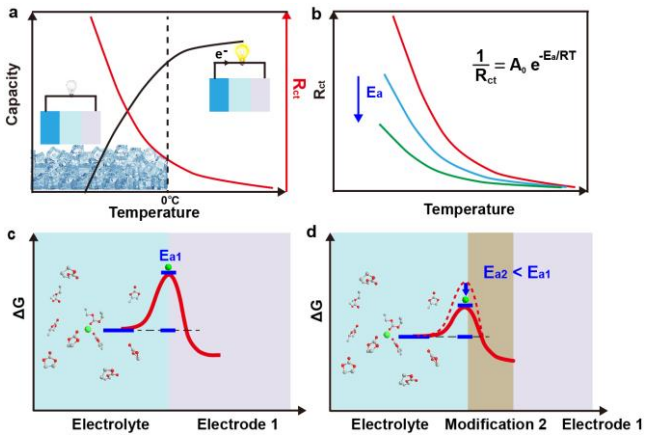

Scheme 1. (a-b) Sluggish interfacial kinetics due to increased R_{ct} for LIB working at low temperatures. (c-d) The proposed design idea to tune energy barrier via controlling surface chemistry.

The concept of surface doping is to endow the electrode with a new interface owning lower energy barrier of the charge transfer process (Scheme 1c,d). Inspired from this, we adopted nickel surface doping for $LiMn_2O_4$ to form the topmost layer with electrochemical activate $LiNi_{0.5-x}Mn_{1.5+x}O_4$, which has a much lower activation energy of charge transfer.[8] Impressively, the modified electrode exhibits a greatly high capacity retention of ~75.4% at 0.2 C (1 C=140 mA/g) even at -30 °C (normalized to that of room temperature), far surpassing the hardly discharged unmodified counterpart. The mechanism behind the superior performance has been uncovered via electrochemical impedance spectroscopy (EIS) and density functional theory calculation (DFT), indicating that nickel surface doping could strengthen the Li binding to surface sites and extraordinarily give rise to a ~20% reduction of the activation energy for the charge transfer process. The insights gathered through controlling surface chemistry to tune energy barrier of interfacial process will advance the comprehension for rational design for LIBs operating under thermal extremes.

Typically, commercial $LiMn_2O_4$ (denoted as LMO) purchased from MTI company was used as core materials for nickel precursor surface coating through a sol-gel method and subsequent heat treatment induced the penetration of nickel atoms into the surface layers of LMO (Figure S1).[9] X-ray diffraction (XRD) was first conducted to characterize the crystal structures of the samples. As displayed in Figure 1a,b, the corresponding XRD patterns re-

vealed the typical diffraction peaks of a well crystallized spinel structure with Fd-3m symmetry, indicating the cubic symmetry of spinel was well maintained after Ni doping. Rietveld analysis of these XRD showed that the lattice parameter of LMO was slightly decreased compared to the unmodified sample (Table S1), which should be aroused by the incorporation of Ni ions into the surface spinel lattice through partially substituting manganese ions of LMO. X-ray absorption near edge structure (XANES) were further carried out to investigate the local environment of Mn and Ni in both samples. As revealed in Figure 1c, LMO-Ni exhibits nearly identical features as the bare LMO, suggesting that bulk spinel structure of LMO is well maintained after the Ni doping. In addition, new-emerged peak and reduced ratio of Mn^{3+} in X-ray photoelectron spectroscopy (XPS) spectra indicate the presence of Ni in the surface layer (Figure S2). The Ni substitution could be further confirmed by Raman scattering (Figure S3) and charging/discharging curves (Figure S4).[10]

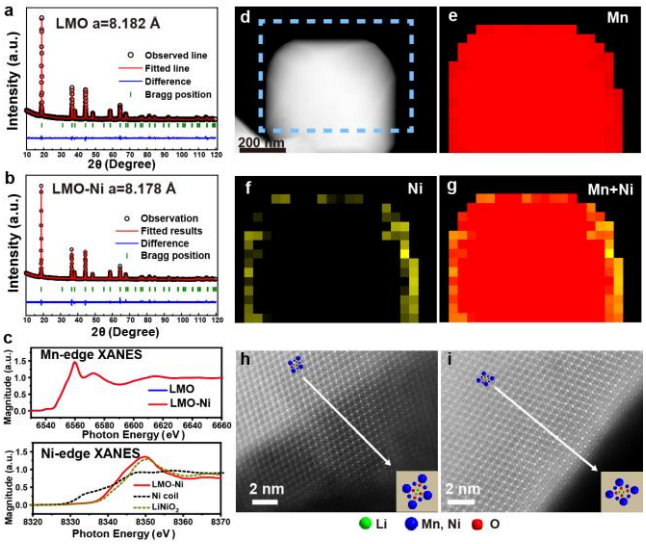

Figure 1. (a-b) XRD patterns and the corresponding Rietveld refinement of LMO (a) and LMO-Ni (b). (c) Mn-edge and Ni-edge XANES. (d) HAADF-STEM image, (e-g) EELS mapping of Mn, Ni and superimposed Mn and Ni for LMO-Ni. (h-i) Aberration-corrected HAADF-STEM images of (h) LMO and (i) LMO-Ni observed along [110] direction.

The morphology of the samples was characterized by scanning electron microscopy (SEM) and transmission electron microscopy (TEM), showing that the particle size remained unchanged after doping (Figure S5). The presence of Ni in the surface was further verified by the electron energy loss spectroscopy (EELS) analysis (Figure S6). As revealed by the elemental mapping on the selected area in Figure 1d-g, the overlay signals of Mn and Ni clearly disclosed that Ni was distributed in the surface. To directly identify the effect of doping on crystallographic structure at the atomic scale, aberration-corrected scanning transmission electron microscopy (STEM) technique was employed, equipped with high-angle annular dark-field (HAADF) detectors.[11] As depicted in Figure 1h,i, both samples displayed the same LMO diamonds correlated to Mn_2O_4 framework without visible atoms occupying the tetrahedral sites, demonstrating that Ni partially displace octahedral-site Mn atoms with the spinel structure well maintained.[12]

In order to study the impact of surface doping on the charge transfer process, coin cells were first assembled using lithium metal as anode and LMO or LMO-Ni as cathode, and then electrochemical impedance spectroscopy (EIS) was adopted to monitor cell impedance at varied temperatures (Figure 2a,b, S7, Table S2). According to the Arrhenius relationship that charge transfer resistance (R_{ct}) follows, the value of activation energy (E_a) of charge transfer process could be obtained from the slope of a $\log(1/R_{ct})$ versus the inverse of temperature (1/T) plot (Figure 2c). As displayed in Figure 2d, the calculated E_a for the LMO and LMO-Ni electrode are about 58.3 and 47.2 kJ/mol, respectively, meaning that Ni surface doping for LMO could impressively give rise to a nearly 20% reduction of the energy barrier for the charge transfer process. This facilitated Li^+ transport across the electrolyte/electrode interface should be attributed to the introduction of Ni and the changed ratio of Mn^{4+}-O^{2-} bond. Other cations including copper, aluminum and titanium were also tried for comparison, which show no such apparent effect. Based on these results as well as the activation energy of diffusion process (Figure S7), the rate-determining step of batteries could be well evaluated by the simulation relying on the Pseudo-Two-Dimensional (P2D) model according to Butler-Volmer equations.[13] As presented by the results in Figure 2e, the predominant performance-limiting factor of bare LMO electrode would switch from the diffusion process to the charge transfer, when the temperature decreased from room temperature to ~10 °C. However, for LMO-Ni electrode, this inflection point was substantially reduced to about -70 °C. In other words, the interfacial issues over broad low-temperature range have been effectively addressed after nickel surface doping, which should be attributed to the remarkably lowered energy barrier for charge transfer process after modified surface chemistry.

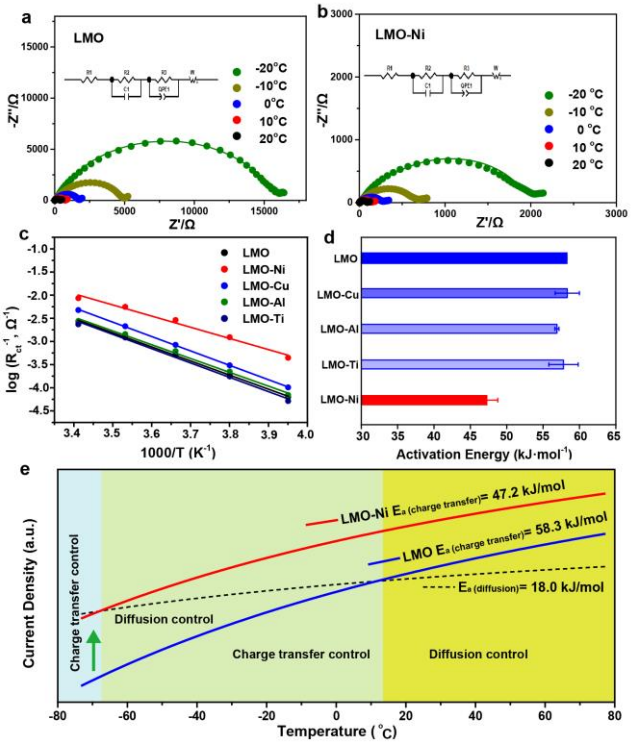

Figure 2. (a-b) Electrochemical impedance spectroscopy (EIS) study of LMO (a) and LMO-Ni (b) at varied temperatures. (c) Arrhenius plot for charge transfer resistance (R_{ct}) and (d) activation energy of charge transfer process of LMO without/with surface doping. (e) Simulation to evaluate the rate-determining step of LMO and LMO-Ni electrode at varied temperatures.

To evaluate the impact of Ni surface doping on the electrochemical performance of LMO, charging/discharging measure-

ments were conducted in an environmental chamber. As shown in Figure 3a, S8, two electrodes deliver a comparable capacity at 0.2 C. But at high rates, the electrochemical performance of LMO-Ni far surpasses the counterpart of LMO, an indicative of enhanced interfacial kinetics after modification. Notably, distinguished from traditional strategies, the improved low-temperature performances are not based on compromising the cycle life at elevated temperatures (Figure 3b). On the contrary, divalent Ni^{2+} substitution markedly enhanced structural stability through pronouncedly reducing Mn^{3+} amount (Figure S9). To well compare performance with decreasing temperatures, current density was fixed at 0.2 C and capacities were normalized by the room-temperature value for clarity. As shown in Figure 3c, the capacity retention at subzero temperatures was dramatically improved after nickel substitution, which could impressively deliver ~90% capacity at -20 °C, far superior to ~65% of bare LMO. Even when it further dipped to -30 °C, LMO-Ni still maintained a capacity retention of ~75.4%, while unmodified LMO could hardly be discharged. Meanwhile, LMO-Ni electrode displayed remarkable rate-performances at -20 °C (Figure 3d,e). In addition, the doping amount of Ni should be controlled within an appropriate range and too much substitution would sacrifice the total available capacity (Figure 3f, S10). In brief, these enhanced low-temperature performances should be attributed to the largely reduced activation energy of charge transfer process induced by the interfacial chemistry change after Ni surface doping.

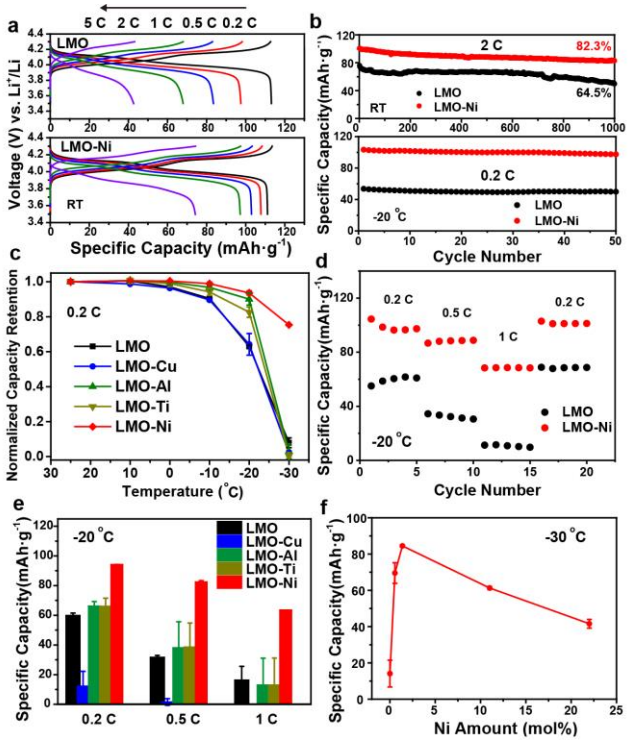

Figure 3. (a) Charging/discharging curves of LMO and LMO-Ni at different current density at room temperature. (b) Cycling performance of LMO and LMO-Ni. (c) Normalized capacity retention of bare and modified LMO with temperature. (d) Rate performance of LMO and LMO-Ni at -20 °C. (e) Specific capacity of bare and modified LMO at various current density at -20 °C. (f) Specific capacity of LMO-Ni with varied amount of nickel at 0.2 C at -30 °C.

To correlate the facilitated charge transfer process with the presence of Ni atoms in the surface, density functional theory (DFT) calculations study of lithium adsorption on the bare and surface modified λ-MnO_2 have been performed,[14] considering that the binding energy of Li to the surface sites has been proved to determine the overall barrier for both lithiation and delithiation.[15] Since XAS and STEM characterizations show that Ni mainly appeared in Mn site the surface layer, we replaced a Mn atom with Ni in MnO_6 group in the LMO-Ni case and the substitution site was found to be energetically favorable (Figure 4a). As presented in Figure 4b, the Li binding energy on the surface was remarkably reduced about ~0.7 eV after nickel doping, demonstrating the Li binding on electrode surface is significantly strengthened after modification (Figure 4c). Moreover, in contrast with other cationic doping (Figure S11, S12), nickel surface doping exhibits positive effects on lithium diffusion (Table S3). So, it's probably that the synergistic effect of strengthened Li binding and promoted lithium diffusion in the topmost layers leads to largely decreased threshold energy of interfacial process.

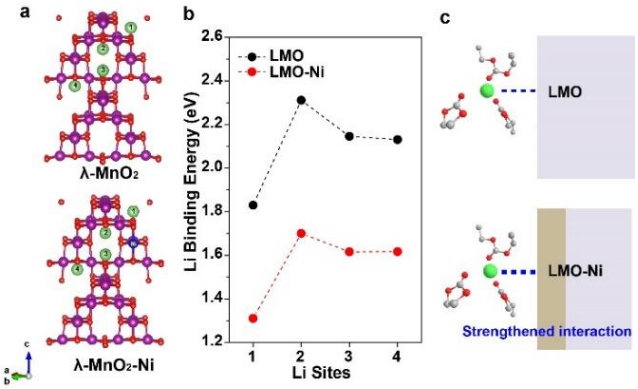

Figure 4. (a) Crystal structures of relaxed bare and Ni-doped λ-MnO_2 (001) surfaces. Red, purple and green spheres represent O, Mn and Li, respectively. (b) Li binding energy on four different adsorption sites of LMO and LMO-Ni. (c) Schematic illustration of strengthened Li binding on electrode surface after Ni doping.

In summary, we demonstrated that surface chemistry tuning via proper cationic doping could be an alternative approach to lower energy barrier of charge transfer process, potentially addressing the interfacial issue for cells operating at low temperatures. These should be attributed to the strengthened Li binding on the surface and promoted lithium diffusion in the topmost layers, verified by the EIS study and DFT calculation. Benefited from these, the model system, nickel surface-doped LMO electrode showed significantly improved capacity retention (~75.4% at -30 °C) and rate-capability (~70 mAh/g at 1 C at -20 °C) at low temperatures, without sacrificing the cyclability and stability. The design of interfacial chemistry provides an effective strategy for LIBs to well survive and operate under thermal extremes.

ASSOCIATED CONTENT

Supporting Information

The Supporting Information is available free of charge on the ACS Publications website. SEM and TEM images; EELS spectra of LMO-Ni; refined lattice parameters; XPS and Raman spectra; charging/discharging curves with different voltage range; rate performance of bare and surface doped LMO; Li^+ diffusion coefficients calculated from EIS; XRD patterns and TEM images after cycle; discharging profiles.

AUTHOR INFORMATION

Corresponding Author

*du_yonghua@ices.a-star.edu.sg
*chenxd@ntu.edu.sg

Notes

The authors declare no competing financial interests.

ACKNOWLEDGMENT

This work was supported by Singapore National Research Foundation (Nanomaterials for Energy and Water Management CREATE Programme), Energy Innovation Research Programme (EIRP) NRF2015EWT-EIRP002-008. The authors are grateful to Dr. Qinghua Liang for XRD refinement and Dr. Yee Yan Tay for STEM characterization. We also thank Drs Renheng Wang, Hongwei Zhang, Shengkai Cao, Jiaqi Wei and Lin Liu for helpful discussion.

REFERENCES

(1) (a) Rodrigues, M.-T. F.; Babu, G.; Gullapalli, H.; Kalaga, K.; Sayed, F. N.; Kato, K.; Joyner, J.; Ajayan, P. M. A materials perspective on Li-ion batteries at extreme temperatures. *Nat. Energy* **2017,** *2*, 8. (b) Bandhauer, T. M.; Garimella, S.; Fuller, T. F. A critical review of thermal issues in lithium-ion batteries. *J. Electrochem. Soc.* **2011,** *158*, 3. (c) Choi, N. S.; Chen, Z.; Freunberger, S. A.; Ji, X.; Sun, Y. K.; Amine, K.; Yushin, G.; Nazar, L. F.; Cho, J.; Bruce, P. G. Challenges facing lithium batteries and electrical double-layer capacitors. *Angew. Chem. Int. Ed.* **2012,** *51*, 40. (d) Nagasubramanian, G. Electrical characteristics of 18650 Li-ion cells at low temperatures. *J. Appl. Electrochem.* **2001,** *31*, 1. (e) Wang, C.-Y.; Zhang, G.; Ge, S.; Xu, T.; Ji, Y.; Yang, X.-G.; Leng, Y. Lithium-ion battery structure that self-heats at low temperatures. *Nature* **2016,** *529*, 7587.

(2) (a) Goodenough, J. B.; Park, K.-S. The Li-ion rechargeable battery: a perspective. *J. Am. Chem. Soc.* **2013,** *135*, 4. (b) Tarascon, J. M.; Armand, M. Issues and challenges facing rechargeable lithium batteries. *Nature* **2001,** *414*, 359. (c) Liu, Y.; Zhou, G.; Liu, K.; Cui, Y. Design of complex nanomaterials for energy storage: past success and future opportunity. *Acc. Chem. Res.* **2017,** *50*, 12. (d) Tang, Y. X.; Zhang, Y. Y.; Li, W. L.; Ma, B.; Chen, X. D. Rational material design for ultrafast rechargeable lithium-ion batteries. *Chem Soc Rev* **2015,** *44*, 17. (e) Liu, Q.; Su, X.; Lei, D.; Qin, Y.; Wen, J.; Guo, F.; Wu, Y. A.; Rong, Y.; Kou, R.; Xiao, X.; Aguesse, F.; Bareño, J.; Ren, Y.; Lu, W.; Li, Y. Approaching the capacity limit of lithium cobalt oxide in lithium ion batteries via lanthanum and aluminium doping. *Nat. Energy* **2018,** *3*, 11. (f) Liu, Y.; Lin, X.-J.; Sun, Y.-G.; Xu, Y.-S.; Chang, B.-B.; Liu, C.-T.; Cao, A.-M.; Wan, L.-J. Precise surface engineering of cathode materials for improved stability of lithium-ion batteries. *Small DOI: 10.1002/smll.201901019*. (g) Zhang, J.-N.; Li, Q.; Ouyang, C.; Yu, X.; Ge, M.; Huang, X.; Hu, E.; Ma, C.; Li, S.; Xiao, R.; Yang, W.; Chu, Y.; Liu, Y.; Yu, H.; Yang, X.-Q.; Huang, X.; Chen, L.; Li, H. Trace doping of multiple elements enables stable battery cycling of $LiCoO_2$ at 4.6 V. *Nat. Energy* **2019,** *DOI: 10.1021/acsami.9b05100*. (h) Piao, J.-Y.; Gu, L.; Wei, Z.; Ma, J.; Wu, J.; Yang, W.; Gong, Y.; Sun, Y.-G.; Duan, S.-Y.; Tao, X.-S.; Bin, D.-S.; Cao, A.-M.; Wan, L.-J. Phase control on surface for the stabilization of high energy cathode materials of lithium ion batteries. *J. Am. Chem. Soc.* **2019,** *141*, 12.

(3) (a) Ji, Y.; Zhang, Y.; Wang, C.-Y. Li-ion cell operation at low temperatures. *J. Electrochem. Soc.* **2013,** *160*, 4. (b) Huang, C. K.; Sakamoto, J.; Wolfenstine, J.; Surampudi, S. The limits of low-temperature performance of Li-ion cells. *J. Electrochem. Soc.* **2000,** *147*, 8. (c) Fan, J.; Tan, S. Studies on charging lithium-ion cells at low temperatures. *J. Electrochem. Soc.* **2006,** *153*, 6. (d) Wang, C.; Appleby, A. J.; Little, F. E. Low-temperature characterization of lithium-ion carbon anodes via microperturbation measurement. *J. Electrochem. Soc.* **2002,** *149*, 6. (e) Abraham, D.; Heaton, J.; Kang, S.-H.; Dees, D.; Jansen, A. Investigating the low-temperature impedance increase of lithium-ion cells. *J. Electrochem. Soc.* **2008,** *155*, 1. (f) Lin, H.-P.; Chua, D.; Salomon, M.; Shiao, H.; Hendrickson, M.; Plichta, E.; Slane, S. Low-temperature behavior of Li-ion cells. *Electrochem. Solid-State Lett.* **2001,** *4*, 6.

(4) (a) Liu, Y.; Yang, B.; Dong, X.; Wang, Y.; Xia, Y. A simple pre-lithiation strategy to build a high-rate and long-life lithium-ion battery with improved low-temperature performance. *Angew. Chem. Int. Ed.* **2017,** *56*, 52. (b) You, Y.; Yao, H. R.; Xin, S.; Yin, Y. X.; Zuo, T. T.; Yang, C. P.; Guo, Y. G.; Cui, Y.; Wan, L. J.; Goodenough, J. B. Subzero-temperature cathode for a sodium-ion Battery. *Adv. Mater.* **2016,** *28*, 33. (c) Yao, J.; Wu, F.; Qiu, X.; Li, N.; Su, Y. Effect of CeO_2-coating on the electrochemical performances of $LiFePO_4$/C cathode material. *Electrochim. Acta* **2011,** *56*, 16. (d) Yuan, T.; Yu, X.; Cai, R.; Zhou, Y.; Shao, Z. Synthesis of pristine and carbon-coated $Li_4Ti_5O_{12}$ and their low-temperature electrochemical performance. *J. Power Sources* **2010,** *195*, 15. (e) Shiao, H.-C. A.; Chua, D.; Lin, H.-p.; Slane, S.; Salomon, M. Low temperature electrolytes for Li-ion PVDF cells. *J. Power Sources* **2000,** *87*, 1-2. (f) Plichta, E. J.; Behl, W. K. A low-temperature electrolyte for lithium and lithium-ion batteries. *J. Power Sources* **2000,** *88*, 2. (g) Stuart, T.; Hande, A. HEV battery heating using AC currents. *J. Power Sources* **2004,** *129*, 2. (h) Qiu, Q.-Q.; Shadike, Z.; Wang, Q.-C.; Yue, X.-Y.; Li, X.-L.; Yuan, S.-S.; Fang, F.; Wu, X.-J.; Hunt, A.; Waluyo, I.; Bak, S.-M.; Yang, X.-Q.; Zhou, Y.-N. Improving the electrochemical performance and structural stability of the $LiNi_{0.8}Co_{0.15}Al_{0.05}O_2$ cathode material at high-voltage charging through Ti substitution. *ACS Appl. Mater. Interfaces* **2019,** *DOI: 10.1021/acsami.9b05100*.

(5) (a) Jow, R.; Zhang, S. S.; Xu, K.; Allen, J. Electrolytes for low temperature operations of Li-ion batteries. *ECS Trans.* **2007,** *3*, 27. (b) Smart, M.; Whitacre, J.; Ratnakumar, B.; Amine, K. Electrochemical performance and kinetics of $Li_{1+x}(Co_{1/3}Ni_{1/3}Mn_{1/3})_{1-x}O_2$ cathodes and graphite anodes in low-temperature electrolytes. *J. Power Sources* **2007,** *168*, 2. (c) Smart, M.; Ratnakumar, B.; Chin, K.; Whitcanack, L. Lithium-ion electrolytes containing ester cosolvents for improved low temperature performance. *J. Electrochem. Soc.* **2010,** *157*, 12. (d) Cho, Y.-G.; Kim, Y.-S.; Sung, D.-G.; Seo, M.-S.; Song, H.-K. Nitrile-assistant eutectic electrolytes for cryogenic operation of lithium ion batteries at fast charges and discharges. *Energy Environ. Sci.* **2014,** *7*, 5. (e) Li, Q.; Jiao, S.; Luo, L.; Ding, M. S.; Zheng, J.; Cartmell, S. S.; Wang, C.-M.; Xu, K.; Zhang, J.-G.; Xu, W. Wide-temperature electrolytes for lithium-ion batteries. *ACS Appl. Mater. Interfaces* **2017,** *9*, 22. (f) Rustomji, C. S.; Yang, Y.; Kim, T. K.; Mac, J.; Kim, Y. J.; Caldwell, E.; Chung, H.; Meng, Y. S. Liquefied gas electrolytes for electrochemical energy storage devices. *Science* **2017,** *356*, 6345.

(6) (a) Yamada, Y.; Iriyama, Y.; Abe, T.; Ogumi, Z. Kinetics of lithium ion transfer at the interface between graphite and liquid electrolytes: effects of solvent and surface film. *Langmuir* **2009,** *25*, 21. (b) Xu, K.; von Cresce, A.; Lee, U. Differentiating contributions to "ion transfer" barrier from interphasial resistance and Li^+ desolvation at electrolyte/graphite interface. *Langmuir* **2010,** *26*, 13. (c) Park, M. H.; Lee, Y. S.; Lee, H.; Han, Y.-K. Low Li^+ binding affinity: An important characteristic for additives to form solid electrolyte interphases in Li-ion batteries. *J. Power Sources* **2011,** *196*, 11. (d) Zhang, S.; Xu, K.; Jow, T. Electrochemical impedance study on the low temperature of Li-ion batteries. *Electrochim. Acta* **2004,** *49*, 7. (e) Zhang, Y.; Malyi, O. I.; Tang, Y.; Wei, J.; Zhu, Z.; Xia, H.; Li, W.; Guo, J.; Zhou, X.; Chen, Z. Reducing the charge carrier transport barrier in functionally layer-graded electrodes. *Angew. Chem. Int. Ed.* **2017,** *56*, 47.

(7) Funabiki, A.; Inaba, M.; Ogumi, Z. Ac impedance analysis of electrochemical lithium intercalation into highly oriented pyrolytic graphite. *J. Power Sources* **1997,** *68*, 2.

(8) (a) Swiderska-Mocek, A.; Lewandowski, A. Kinetics of Li-ion transfer reaction at $LiMn_2O_4$, $LiCoO_2$, and $LiFePO_4$ cathodes. *J. Solid State Electrochem.* **2017,** *21*, 5. (b) Jow, T. R.; Marx, M. B.; Allen, J. L. Distinguishing Li^+ charge transfer kinetics at NCA/electrolyte and graphite/electrolyte Interfaces, and NCA/electrolyte and LFP/electrolyte interfaces in Li-ion cells. *J. Electrochem. Soc.* **2012,** *159*, 5. (c) Tang, Y.; Deng, J.; Li, W.; Malyi, O. I.; Zhang, Y.; Zhou, X.; Pan, S.; Wei, J.; Cai, Y.; Chen, Z. Water-soluble sericin protein enabling stable solid–electrolyte interphase for fast charging high voltage battery electrode. *Adv. Mater.* **2017,** *29*, 33.

(9) (a) Zhang, W.; Chi, Z. X.; Mao, W. X.; Lv, R. W.; Cao, A. M.; Wan, L. J. One-nanometer-precision control of Al_2O_3 nanoshells through a solution-based synthesis route. *Angew. Chem. Int. Ed.* **2014,** *53*, 47. (b) Piao, J.-Y.; Sun, Y.-G.; Duan, S.-Y.; Cao, A.-M.; Wang, X.-L.; Xiao, R.-J.; Yu, X.-Q.; Gong, Y.; Gu, L.; Li, Y. Stabilizing cathode materials of lithium-ion batteries by controlling interstitial sites on the surface. *Chem* **2018,** *4*, 7.

(10) Wei, Y.; Yan, L.; Wang, C.; Xu, X.; Wu, F.; Chen, G. Effects of Ni doping on [MnO_6] octahedron in $LiMn_2O_4$. *J. Phys. Chem. B* **2004,** *108*, 48.

(11) Xiao, B.; Liu, H.; Liu, J.; Sun, Q.; Wang, B.; Kaliyappan, K.; Zhao, Y.; Banis, M. N.; Liu, Y.; Li, R. Nanoscale manipulation of spinel lithium nickel manganese oxide surface by multisite Ti occupation as high-performance cathode. *Adv. Mater.* **2017,** *29*, 47.

(12) Lin, M.; Ben, L.; Sun, Y.; Wang, H.; Yang, Z.; Gu, L.; Yu, X.; Yang, X.-Q.; Zhao, H.; Yu, R. Insight into the atomic structure of high-voltage spinel $LiNi_{0.5}Mn_{1.5}O_4$ cathode material in the first cycle. *Chem. Mater.* **2014,** *27*, 1.

(13) Torchio, M.; Magni, L.; Gopaluni, R. B.; Braatz, R. D.; Raimondo, D. M. Lionsimba: a matlab framework based on a finite volume model suitable for Li-ion battery design, simulation, and control. *J. Electrochem. Soc.* **2016,** *163*, 7.

(14) (a) Kresse, G.; Furthmüller, J. Efficiency of ab-initio total energy calculations for metals and semiconductors using a plane-wave basis set. *Comput. Mater. Sci.* **1996,** *6*, 1. (b) Kresse, G.; Joubert, D. From ultrasoft pseudopotentials to the projector augmented-wave method. *Phys. Rev. B* **1999,** *59*, 3.

(15) (a) Dathar, G. K. P.; Sheppard, D.; Stevenson, K. J.; Henkelman, G. Calculations of Li-ion diffusion in olivine phosphates. *Chem. Mater.* **2011,** *23*, 17. (b) Maxisch, T.; Zhou, F.; Ceder, G. Ab initio study of the migration of small polarons in olivine Li_xFePO_4 and their association with lithium ions and vacancies. *Phys. Rev. B* **2006,** *73*, 10.

For Table of Contents Only